MSDE

PAPER

Designing stable bimetallic nanoclusters *via* an iterative two-step optimization approach†

Xiangyu Yin,[a] Natalie M. Isenberg,[a] Christopher L. Hanselman,[a] James R. Dean,[b] Giannis Mpourmpakis [iD][b] and Chrysanthos E. Gounaris [iD] *[a]

Determining the energetically most favorable structure of nanoparticles is a fundamentally important task towards understanding their stability. In the case of bimetallic nanoclusters, their vast configurational space makes it especially challenging to find the global energy optimum *via* experimental or computational screening. To that end, this work proposes a two-step optimization-based design framework to address this hard combinatorial problem. Given a nanocluster of fixed shape, a rigorous mixed-integer linear programming model is formulated based on a bond-centric cohesive energy function to identify the most cohesive bimetallic configuration for a given composition. This capability is coupled with a metaheuristic strategy that searches over the space of nanocluster shapes to obtain optimal structures. We apply our proposed methodology on AgCu, AuAg and CuAu systems, quantifying how the size and composition of a nanocluster influences its overall cohesion. Furthermore, we observe various synergistic effects between Cu and Au in promoting cohesive energy, while multiple segregation patterns are identified in all three studied binary systems. Our methodology serves as an efficient computational tool for investigating bimetallic nanoclusters stability properties as well as provides model nanoclusters for further investigations.

Design, System, Application

Bimetallic nanoclusters exhibit interesting properties that make them attractive for a wide variety of application contexts. To that end, the identification of stable bimetallic nanocluster designs of various sizes and compositions is an important first step to enable a multitude of rigorous investigations involving such materials. However, even for a fixed particle size, the design space of a bimetallic nanocluster is highly complex, as the combinatorics of shape selection compound with that of chemical ordering. In this manuscript, we develop a computational framework to identify highly cohesive bimetallic nanocluster designs of various particle sizes and composition ratios. Starting from monometallic nanoclusters obtained *via* a previously proposed shape optimization approach, we develop a hybrid "structure-first-order-second" decomposition that enables the efficient exploration of the full design space. In particular, a metaheuristic search optimization algorithm is tasked with identifying promising nanocluster shapes, iteratively improving upon those, while a mixed integer linear programming-based algorithm complements the former to identify optimal chemical orderings in light of given shapes. Comprehensive computational studies on AuAg, AgCu and CuAu nanoclusters reveal highly cohesive configurations as well as instances of alloyed clusters that possess greater cohesive energy than their monometallic counterparts.

1 Introduction

Sub-nanometer transition metal clusters exhibit unique catalytic, magnetic, electronic, and optical properties. They are promising materials in a wide range of next-generation technological advances, such as catalysis, electronics, and optics, among others.[1] Compared with their monometallic

[a] Department of Chemical Engineering, Carnegie Mellon University, USA. E-mail: gounaris@cmu.edu
[b] Department of Chemical and Petroleum Engineering, University of Pittsburgh, USA

† Electronic supplementary information (ESI) available: Atomic coordinates for optimal nanocluster structures are available in the ESI. See DOI: 10.1039/d1me00027f

counterparts, bimetallic nanoclusters have unique advantages, including improved performance and cost reduction. In addition, special additive and synergistic effects between the two metals may be achieved *via* tuning the particle's size, shape, composition, and chemical ordering.[2] The flexible design space of bimetallic nanoclusters, combined with growing synthesizing capability to near-atomic precision, motivates the research to identify optimal nano-configurations for target functionalities.

Among all desirable functionalities, stability is of fundamental importance to nanocluster research. Determining energetically favorable nanocluster configurations has attracted particular research interest in understanding stability and other equilibrium properties at low temperatures.[3] This is a hard problem, given the vast combinatorial design space afforded by

the applicable lattice geometries. For a given number N of atoms, the number of unique geometrical isomers is estimated as $O(e^N)$.[4] In the case of bimetallic nanoclusters, the complexity increases further due to the existence of homotops, that is, clusters with the same geometry and composition but featuring different chemical ordering.[5] Consider that, even if a specific cluster shape is assumed, there are still $\mathcal{O}(N!)$ possible ways of labeling it using two atomic identities. The configurational space caused by isomers and homotops makes it impossible to screen every possible nanocluster configuration. Therefore, it is essential to devise efficient algorithms to guide the optimization over such complex design spaces.

In the literature, various metaheuristic methods, such as genetic algorithms, particle swarm optimization, and basin-hopping have been utilized along with empirical or *ab initio* potential energy functions to identify the energetically most favorable nanoclusters.[6–11] Those methods sample the design space randomly or semi-randomly for better solutions and terminate after some stopping criterion – often an arbitrary computation time limit – is met. Although highly stable nanoclusters may be discovered by those approaches, the underlying methods lack the ability to provide a metric of solution optimality. Furthermore, the performance of metaheuristic methods is profoundly sensitive to hyper-parameter settings, calling for a careful tuning effort before they can be applied. In contrast to the above methods, one can utilize mathematical optimization to explore the design space more systematically. The main benefit of this approach is that, once we formulate the design problem as a formal optimization model, we can employ established numerical algorithms and powerful commercial implementations to obtain optimal designs. This approach has been illustrated in the design of transition metallic surfaces,[12,13] doped perovskites,[14] and monometallic nanoclusters,[15] in which the design of transition-metal based nanostructured materials was modeled in the form of a mixed-integer linear program (MILP), a well-known class of optimization models. Notably, in contrast to methods based purely on meta-heuristics, an MILP-based approach offers the ability to determine the incumbent solution's quality, including whether or not this solution is the globally optimal one in light of the objective metric of choice, as well as how far it can be from the anticipated global optimum. With such guarantees, those previous studies were able to discover various non-intuitive designs and interesting trends. The downside of a mathematical optimization approach is their generally poor tractability when addressing highly complex combinatorial design spaces, limiting the size of the particles, or the unit cells of periodic structures, that can be designed in this way.

A highly complex combinatorial design space arises, for example, when one seeks to design bimetallic nanoclusters, where the degrees of freedom associated with the shape and size of the particles are compounded by the possible identities of each of their atoms, as dictated by the applicable composition limits. To that end, we propose in this work a hybrid optimization approach that integrates mathematical optimization and metaheuristic search to alleviate the complexity challenges and identify highly stable bimetallic nanoclusters that are globally optimal in light of the stability function one postulates. Conceptually, the optimization model we seek to solve can be cast as follows:

$$\begin{aligned}
\underset{d \in D}{\text{maximize}} \quad & \text{Stability}(d) \\
\text{subject to} \quad & \text{Size}(d) = N_1 + N_2 \\
& \text{Composition}(d) = \begin{bmatrix} N_1 \\ N_2 \end{bmatrix},
\end{aligned}$$

where variable d abstractly encodes the cluster design, D represents the associated design space, while N_1 and N_2 are the specified number of atoms for each of the cluster's two elements.

To instantiate a formal design model using the above conceptual formulation as the basis, a relationship between a specific configuration d and its stability is needed. Multiple energetic descriptors can be employed to approximate the thermodynamic stability of metal nanoparticles,[16] with the surface energy of the particle being a popular consideration. However, recognizing that subsurface atoms and their chemical ordering plays an important role in the stability of the small bimetallic clusters we are targeting to design in this work, we have chosen to instead focus on a cluster's cohesive energy as a metric of its stability. To that end, in order to find the most stable configuration of such a cluster, we will seek to maximize its cohesive energy, subject to constraints on its size and composition. Here, we select the simple, yet sufficiently accurate, bond-centric (BC) cohesive energy function, which has been shown to predict cohesive energies in good agreement with density functional theory (DFT) calculations for a wide range of binary alloy clusters.[17] Note how, in our context, the BC model can be viewed as the structure–function relationship of interest.

Another important aspect of instantiating a specific design problem is the choice of the design canvas, which corresponds to the superstructure of possible lattice locations that atoms might occupy in any given design. For crystalline materials, such as the nanoclusters contemplated in this work, the geometry may be described with standard Bravais lattices. In the computational investigations of this paper, we shall utilize the face-centered cubic (FCC) lattice as a representative canvas geometry *via* which to illustrate our design framework, but we highlight that our developed design methodology is generic and can be easily adapted to other lattice types. Choosing the geometry and the expanse of the canvas is often at the discretion of the modeler, but these choices should not be entirely arbitrary, as they could affect model accuracy and numerical tractability. For example, the choice of a canvas geometry that is not consistent with the specific chemistry (*i.e.*, metal species) of interest, or the choice of a small canvas compared to the target size of the nanocluster, could over-constrain the problem and lead to erroneous results. At the same time, an overly large canvas

could make the optimization problem harder to solve due to the much larger combinatorial complexity.

The remainder of the manuscript is organized as follows. In section 2, we briefly introduce the BC model for bimetallic cluster cohesive energy evaluation. Using this model as the basis for evaluating stability, we present in section 3 our optimization-based methodology for the identification of highly cohesive particle designs. In section 4, we present our computational studies to derive stable nanocluster designs, and we analyze the latter to elucidate the impact of size, shape, and composition on a nanocluster's stability and equilibrium segregation patterns. We then conclude with some final remarks in section 5.

2 Bond-centric cohesive energy model for bimetallic nanoclusters

The cohesive energy, E_{coh}, is defined as the energy difference between infinitely separated neutral metal atoms and the crystalline cluster formed by those atoms.[18] It measures the average strength of interatomic bonding, thus indicating the overall stability of a nanocluster. By identifying the most cohesive bimetallic nanocluster, we essentially obtain the thermodynamically most stable bimetallic nanoclusters configurations at low temperatures.

The following bond-centric cohesive energy function[17] is utilized as the structure–function relationship in this work.

$$E_{coh} = \frac{1}{N} \sum_{(i,j)\in\mathcal{B}} be_{ij} \tag{1}$$

$$be_{ij} = \frac{\gamma_{k\ell} E_{coh,k}^{bulk}}{\sqrt{CN_k^{bulk}}\sqrt{CN_i}} + \frac{\gamma_{\ell k} E_{coh,\ell}^{bulk}}{\sqrt{CN_\ell^{bulk}}\sqrt{CN_j}} \quad \forall (i,j)\in\mathcal{B} \tag{2}$$

Given the number of atoms, N, and the complete set of bonds, $\mathcal{B}$, eqn (1) describes the per-atom cohesive energy E_{coh} of the particle as the summation of each bond i–j's contribution, be_{ij}, to the overall cohesion, while eqn (2) assumes that such bond contributions only depend on the bonding atoms' coordination numbers, CN_i and CN_j, and their elemental types, k and ℓ, respectively for atoms i and j. In regards to the various parameters, $E_{coh,m}^{bulk}$ is the bulk cohesive energy and CN_m^{bulk} is the bulk coordination number of a metal of type m (where m is either k or ℓ in the above formula). The weighting parameters $\gamma_{k\ell}$ and $\gamma_{\ell k}$ are introduced so as to differentiate contributions from two types of metal atoms in heterolytic bonds. We note that, when $\gamma_{k\ell} = \gamma_{\ell k} = 1$, this bond-centric function reduces to the well-established square root bond-cutting cohesive energy function.[19] The cohesive energy's dependence on the coordination number can be explained by the inherent nearsightedness in transition metals, where perturbations beyond one lattice constant are dampened.[20]

The above bond-centric model is reported to provide promising cohesive energy predictions in a wide range of binary nanoalloy systems using only a small set of parameters and minimal DFT calculations.[17] Its two key parameters, $\gamma_{\ell k}$ and $\gamma_{k\ell}$, depend on dimer bond dissociation energies and can be calculated by solving the following system of equations:

$$\gamma_{\ell k}BDE_{\ell-\ell} + \gamma_{k\ell}BDE_{k-k} = 2BDE_{k-\ell} \tag{3}$$

$$\gamma_{\ell k} + \gamma_{k\ell} = 2, \tag{4}$$

where $BDE_{\ell-\ell}$, BDE_{k-k}, and $BDE_{k-\ell}$ are the dimer bond dissociation energies of the homolytic bonds ℓ–ℓ and k–k, and the heterolytic bond k–ℓ, respectively; these energies can be obtained from either computational or experimental sources. We note that the underlying assumption of this calculation is that the dimer bond dissociation energy trends match bulk cohesive energy trends, which means the bond-centric model can capture around 85% percent of transition metal alloys (298 bimetallic nanoalloys out of all 353 possible binary alloys).[17] In addition to describing stability of bimetallic nanoparticles, this function has also been successfully used as a descriptor for chemical adsorption on the surface of bimetallic nanoparticles.[21]

3 Optimization-based design framework

As discussed, the inherent complexity of bimetallic nanoclusters' design space brings challenges for any effort to rigorously optimize their configuration. The need to decide on both the presence and type of atoms at each and every site leads to many combinations of otherwise feasible decisions. To that end, we develop here a two-step solution approach, which we refer to as a "structure-first-order-second" strategy. As its name suggests, the existence of atoms within the design canvas is first determined without consideration of the types of atoms at each location. Then, with the shape of the nanocluster considered fixed, the metal type identities of the atoms that exist in the provisional design are decided afterwards (i.e., chemical ordering). The two searches are integrated in an outer-inner loop scheme, which proceeds until convergence to an optimal structure is reached. With this approach, we are essentially decomposing the full problem into two less complex sub-problems that are more manageable to address. A similar strategy of identifying structures without type labels to inform bimetallic nanocluster discovery was also adopted in a recent study of Pt–Co systems.[22]

The remainder of this section discusses our approach in more detail. More specifically, in section 3.1, we present a rigorous mixed-integer linear programming (MILP) optimization model for identifying the chemical ordering of a particle of given shape and composition that maximizes its cohesive energy as per the bond-centric model of section 2. In section 3.2, we discuss how this capability can be embedded in a two-step search approach to optimize over the

space of particle configurations using metaheuristic search algorithms described in section 3.3.

3.1 Optimal chemical ordering model

Let a bimetallic nanocluster of given size (*i.e.*, number of atoms N), composition (*i.e.*, partitioning of N into N_1 and N_2, the number of atoms of each its two elements), and shape (*i.e.*, set of bonds connecting the atoms). We denote with $\mathcal{I}$ the set of all locations in this nanocluster, while for each location $i \in \mathcal{I}$, we denote with $\mathcal{I}_i \subset \mathcal{I}$ all neighboring locations that are connected with i *via* an atom–atom bond.

Given this setting, we define binary decision variables x_{ik} to indicate the presence/absence of a particular type-k atom at each location i. More specifically, if $x_{ik} = 1$, a type k atom exists at canvas location i; otherwise, when $x_{ik} = 0$, the site i does not contain a type k atom (and rather contains an atom of the other element $\ell \neq k$). The search for the best design, d^*, is then equivalent to identifying an optimal set of decision variables x^*_{ik}. Additionally, we define binary variables $z_{ijk\ell}$ to represent the existence of a bond between atom types k and ℓ that are respectively placed in locations i and j. Finally, auxiliary continuous variables be_{ij} are utilized to represent the bond $(i–j)$'s contribution to the overall cohesion. Eqn (5) through (12) constitute the complete optimization model.

$$\underset{x_{ik},z_{ijk\ell},\text{be}_{ij}}{\text{maximize}} \frac{1}{N_1 + N_2} \sum_{i \in \mathcal{I}} \sum_{j \in \mathcal{I}_i} \frac{1}{2} \text{be}_{ij} \qquad (5)$$

$$\text{subject to} \sum_{i \in \mathcal{I}} x_{ik} = N_k \quad \forall k \in \{1, 2\} \qquad (6)$$

$$\sum_{k=1}^{2} x_{ik} = 1 \quad \forall i \in \mathcal{I} \qquad (7)$$

$$\{x_{ik} \wedge x_{j\ell}\} \Leftrightarrow z_{ijk\ell} \quad \forall \ell \in \{1, 2\} \quad \forall k \in \{1, 2\} \quad \forall j \in \mathcal{I}_i \quad \forall i \in \mathcal{I} \qquad (8)$$

$$\text{be}_{ij} = \sum_{k=1}^{2} \sum_{\ell=1}^{2} \left(\frac{\gamma_{k\ell} E_{\text{coh},k}^{\text{bulk}}}{\sqrt{\text{CN}_k^{\text{bulk}}} \sqrt{|\mathcal{I}_i|}} + \frac{\gamma_{\ell k} E_{\text{coh},\ell}^{\text{bulk}}}{\sqrt{\text{CN}_\ell^{\text{bulk}}} \sqrt{|\mathcal{I}_j|}} \right) z_{ijk\ell} \qquad (9)$$

$$\forall j \in \mathcal{I}_i \quad \forall i \in \mathcal{I}$$

$$x_{ik} \in \{0, 1\} \quad \forall k \in \{1, 2\} \quad \forall i \in \mathcal{I} \qquad (10)$$

$$z_{ijk\ell} \in \{0, 1\} \quad \forall \ell \in \{1, 2\} \quad \forall k \in \{1, 2\} \quad \forall j \in \mathcal{I}_i \quad \forall i \in \mathcal{I} \qquad (11)$$

$$\text{be}_{ij} \in \mathbb{R}_+ \quad \forall j \in \mathcal{I}_i \quad \forall i \in \in \mathcal{I} \qquad (12)$$

As shown in eqn (5), the model's objective is to maximize the cohesive energy, as the latter is calculated by the bond-centric model, normalized per atom of the particle to readily facilitate comparisons among designs of different sizes. Eqn (6) specify the cluster composition, while eqn (7) ensure that exactly one atom type is designated per each location i. Then, eqn (8) dictate the logic defining the auxiliary variables $z_{ijk\ell}$. The latter are then referenced in eqn (9), which evaluate be_{ij}, *i.e.*, the contribution of each bond $i–j$ to the total cohesive energy. We remark that only the appropriate one out of four possible atom type pairs $k–\ell$, namely the one for which $z_{ijk\ell} = 1$ (or equivalently, the one for which $x_{ik} = 1$ and $x_{j\ell} = 1$ at the same time) will contribute to the right-hand side summation; thus, by summing across all possibilities for atom type assignments, we essentially retrieve bond $i–j$'s contribution to the objective function in variable be_{ij}. Note how, in eqn (9), the cardinalities of sets $\mathcal{I}_i$ correspond to the applicable coordination number of the atom occupying each location i. Finally, eqn (10) and (11) declare the binary nature of decision variables x_{ik} and $z_{ijk\ell}$, respectively, while eqn (12) declare the intermediate quantities be_{ij} as non-negative continuous variables.

In order to formulate a model of MILP form, the logical constraints (eqn (8)) need to be first equivalently transformed into their linear counterparts using the well-known Glover linearization technique, resulting into the following constraints (eqn (8′)).

$$\left. \begin{array}{l} z_{ijk\ell} \leq x_{ik} \\ z_{ijk\ell} \leq x_{j\ell} \\ z_{ijk\ell} \geq x_{ik} + x_{j\ell} - 1 \end{array} \right\} \forall \ell \in \{1, 2\} \quad \forall j \in \mathcal{I}_i \quad \forall k \in \{1, 2\} \quad \forall i \in \mathcal{I} \qquad (8′)$$

The reformulated model can now be instantiated and solved by well-established MILP solvers. More specifically, to do so for a given system of interest, the modeler has to define: (1) the nanocluster shape, namely the locations $\mathcal{I}$ and their bond connectivity $\mathcal{I}_i$ for all $i \in \mathcal{I}$; (2) the applicable metal types and overall cluster composition, N_1 and N_2, as well as collect bulk cohesive energies and calculate parameters $\gamma_{k\ell}$ and $\gamma_{\ell k}$ from dimer bond dissociation energies. We highlight how the above model is presented generically and independently of lattice type. In particular, it is implied that the sets $\mathcal{I}$ and $\mathcal{I}_i$ have been chosen consistently with the lattice geometry one expects to apply given the chemistry of interest. For example, if one targets the design of FCC clusters, one should choose sets that encode FCC patterns, and should do so similarly for any other lattice geometries.

If solved to algorithmic termination by a suitable MILP solver, this bimetallic nanocluster chemical ordering model can provide the mathematically guaranteed global optimal solution, up to the accuracy imposed by the bond-centric model. This optimal solution would then correspond to the most cohesive bimetallic design for a given shape, size, and bimetallic system composition. In this work, we solved our model instances using one of the most popular commercially-available MILP solvers, namely CPLEX version 12.9.[23]

Our experience suggests that the numerical tractability of this model is very good, as we were able to reliably obtain

548 | *Mol. Syst. Des. Eng.*, 2021, **6**, 545–557

This journal is © The Royal Society of Chemistry and IChemE 2021

provable optimal solutions within seconds of CPU time and for systems with up to several hundreds of atoms. Hence, the above model is deemed amenable to serve as the evaluator of an iterative algorithm searching in the space of nanocluster shapes at an outer loop.

3.2 Two-step solution strategy

Before we present our proposed solution strategy, we would like to remark that we conducted extensive investigations using a full-space MILP model that attempted to co-optimize directly on the space of shapes and homotops, *i.e.*, to simultaneously determine the presence of atoms on a lattice superstructure as well as the types of atoms in each occupied location. However, the observed numerical tractability of such a full-space model was not promising. More specifically, for many of the instances under consideration and across a wide range of nanocluster sizes and compositions, attempting to solve the full-space model monolithically using the state-of-the-art CPLEX code did not yield algorithmic termination in a reasonable amount of time. In particular, we found that the solver could not always converge to a provably globally optimal solution before the CPU time limit of one hour, while instead the solver returned feasible solutions with optimality gaps that in some cases exceeded 100%, which means that the true global optimum cluster could have featured more than double the cohesive energy of the solution at hand. Furthermore, by inspecting the bimetallic nanocluster designs corresponding to those feasible solutions, we observed a high degree of randomness in terms of nanocluster shapes and chemical ordering, which suggests that the feasible solutions obtained by the solver at the imposed time limit were not the optimal solutions we were looking for.

These empirical observations led us to pursue a "structure-first-order-second" two-step computational strategy to overcome these limitations. As discussed, the main idea is to decompose the bimetallic nanocluster design problem into a shape optimization step and an chemical ordering step, integrating the two steps in an iterative co-optimization process. Another benefit brought by this strategy is that the shape optimization step can leverage previously developed capabilities for the design of stable monometallic nanoclusters.[15] More specifically, the work of ref. 15 has demonstrated how an MILP model can be used to design monometallic nanoclusters of given size that maximize their dimensionless cohesive energy, $\overline{E^{coh}} := E^{coh}/E^{coh}_{bulk}$. We note here that the work of ref. 15 utilizes the square root bond-cutting (SRBC) cohesive energy function as the objective of focus. However, since this metric does not account for the differences in interactions between different elemental types, it cannot be applied to optimizing chemical ordering, which is why we have chosen the bond-centric cohesive energy function instead. Regardless, the highly cohesive shapes that stem from the use of the SRBC model can still be considered as candidates for bimetallic particle shapes. To that end, by

employing an MILP code like CPLEX on the monometallic design model, one may obtain a hierarchy of P optimal solutions (a.k.a. a solution pool) that consist of the distinct nanocluster shapes featuring cohesive energies from the highest to the Pth-highest possible values. Here, P is a predefined small integer that constitutes an algorithmic parameter (we will later select the value of $P = 20$). All the shapes in this hierarchy are collected as they are likely to exhibit a high degree of cohesiveness in a bimetallic setting as well, and whereas the shape corresponding to the most cohesive monometallic cluster might not be the one corresponding to the most cohesive bimetallic cluster, the latter is likely to be found among those in this solution pool.

At a first pass, one may select any and all of the designs from this solution pool, use it to define the set of locations $\mathcal{I}$, and apply the chemical ordering MILP model introduced in the previous section to rigorously search over the space of bimetallic homotops corresponding to the same particle shape. Below, we propose an efficient workflow for an integrated two-step decision-making process whereby the provisional shape is iteratively updated based on some metaheuristic search algorithm and the chemical ordering model is successively applied to optimize across all corresponding homotops, leading to an improved design that features highest cohesive energy. We remark that the iterative scheme might not reach a globally optimal solution with respect to both shape and ordering; however, as we will demonstrate later in our computational studies, the two-step solution strategy that utilizes a purpose-built metaheuristic search algorithm is able to identify highly cohesive bimetallic designs.

The overall two-step optimization process is synopsized in Fig. 1. Given specifications for the target nanocluster size and composition, as well as given applicable values for all atom type-related parameters, the process begins by obtaining the pool of the P most cohesive monometallic nanocluster shapes from the work of ref. 15. Using each of the shapes as the input, we apply the above presented chemical ordering MILP model to obtain the best possible bimetallic nanocluster design conforming to each given shape. By comparing all such designs, we pick the one with the highest cohesive energy as our initial design.

However, the shapes represented in the pool of highly cohesive monometallic nanoclusters might not contain the optimal shape for a bimetallic cluster. To that end, we expand our search effort to the full space of cluster shapes by utilizing a purpose-built metaheuristic search process that is detailed in the next subsection of this paper. For any new shape iterate that is postulated *via* this process, we apply again our MILP model to evaluate its cohesiveness in light of the optimal chemical ordering afforded by this shape. The process iterates until we reach some termination condition, which could be a limit on the CPU time and/or iterations through the loop or a detection that the solution progress has stagnated (*e.g.*, not having identified a better design within a predefined number of recent iterations).
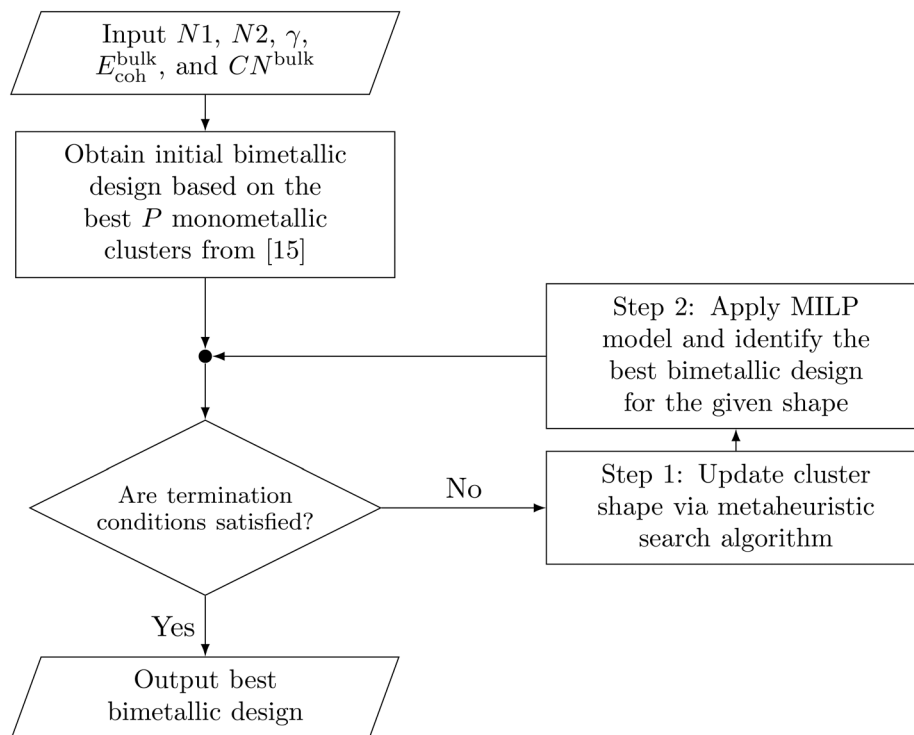
This journal is © The Royal Society of Chemistry and IChemE 2021

Mol. Syst. Des. Eng., 2021, **6**, 545–557 | **549**

Fig. 1 Two-step solution strategy for the identification of highly cohesive bimetallic nanoclusters.

3.3 Metaheuristic search for optimal cluster shapes

Given early bimetallic designs, as obtained by optimizing chemical ordering of nanoclusters that are known to be highly cohesive as monometallics, we can now apply an appropriate, purpose-built metaheuristic search algorithm to improve those designs further. Metaheuristic search is an optimization paradigm that aims to iteratively modify provisional solutions according to a suitably defined local neighborhood, which constitutes a direction of search in the problem's decision space, into potentially better solutions.[24,25] Proper strategies to initialize solutions, modify existing solutions, decide the acceptance or not of new solutions, and terminate the search are essential for designing efficient metaheuristic search algorithms. There exist a lot of algorithmic frameworks that follow this paradigm of search, including genetic algorithms, simulated annealing, variable neighborhood search, ant colony optimization and particle swarm optimization, to name but a few.[26] As also mentioned in the introduction, however, metaheuristic search algorithms provide no optimality proof at termination. Hence, selecting a scheme that is found to perform efficiently in each application and properly tuning its hyperparameters, is important. There in fact exists a lot of prior work that utilizes such methods to search for stable nanoclusters.[6–11] Our algorithm differs from the literature work in the sense that each iterate in our search constitutes a large collection of bimetallic designs to include all possible homotops, the best of which is selected after optimizing the chemical ordering *via* the MILP model presented earlier. In effect, our proposed approach may also be classified as a

matheuristic algorithm,[27,28] which to the best of our knowledge, constitutes the first employment of such an algorithm in the context of designing nanostructured materials.

After some numerical experimentation with other options, we decided to pursue the development of a simulated annealing (SA) scheme to guide the search in terms of particle shapes. The SA scheme is inspired by the annealing process followed in metallurgy, where heating and controlled cooling are coupled to improve material properties. In an SA guided search, improving solutions are always accepted, while worsening solutions are accepted with specific probabilities. A parameter T (mimicking the temperature that constantly drops in the real annealing process) determines those probabilities *via* a Boltzmann factor. Initially, the parameter T is larger, enabling more frequent acceptances of worsening local search moves to diversify the search, but as the search progresses, T decreases and the likelihood of accepting worsening solutions diminishes, intensifying the search around the locally applicable optimum. In essence, at each iteration the algorithm evolves across the spectrum from random sampling (accepting all moves) to greedy search (only accepting improving modifications). The initial temperature setting and the rate of cooling are hyperparameters that require careful tuning, while a search trajectory may undergo multiple cycles of cooling followed by subsequent reheating to the initial temperature. For further details on how to set up an efficient SA implementation, we refer interested readers to a multitude of literature on the topic (see, *e.g.*, ref. 26 and 29).

The local moves applied during each SA iteration are proposed based on the applicable neighborhood of search, which is usually purposely defined in each application. In our case, we define this neighborhood as the repositioning of a single surface atom. We focus on repositioning only surface atoms due to the underlying hypothesis that the less coordinated surface atoms will have a more significant impact on the cohesive energies. Furthermore, it is important to highlight that this specific neighborhood of search does not restrict the accessible search space, as all transitions from any shape to any other shape can be achieved *via* successive single surface atom repositionings. After each surface atom repositioning, the CPLEX code is applied to re-determine the chemical ordering that is most cohesive in light of all homotops of the new shape. Indeed, the ability to consider all homotops at once reduces the number of needed iterations and improves search efficiency compared to a less sophisticated implementation that would have incorporated atom labeling as part of the SA neighborhood definition.

4 Computational results

Three bimetallic systems, namely AuAg, AgCu and CuAu are chosen based on the assumption that they tend to form at equilibrium face centered cubic (FCC) crystalline solids, where $CN^{bulk} = 12$. Bulk cohesive energies, as found in literature for the three types of metals involved, are taken as $E_{coh,Au}^{bulk} = 3.81$ eV, $E_{coh,Cu}^{bulk} = 3.49$ eV, and $E_{coh,Ag}^{bulk} = 2.95$ eV.[30] Weighting parameters are calculated *via* eqn (3) and (4), using dimer bond dissociation energies obtained from experimental data in the literature.[31] The applicable parameters are $\gamma_{AuAg} = 1.281$ and $\gamma_{AgAu} = 0.719$ for the AuAg system, $\gamma_{AgCu} = 1.389$ and $\gamma_{CuAg} = 0.611$ for the AgCu system, and $\gamma_{CuAu} = -0.357$ and $\gamma_{AuCu} = 2.357$ for the CuAu system.

For each of these bimetallic systems of interest, we consider a particle size range N between 6 and 65, as well as all applicable compositions from pure metal type A to pure metal type B. In total, we consider 6570 different test instances that were generated for these computational experiments. The exact atomic coordinates of all optimal structures are provided as *XYZ* files in the ESI.† In the remainder of the paper, a unique combination of size, composition, and bimetallic system is referred to as A_mB_n, where A and B are the metal species, while m and n are the number of atoms for each respective type.

4.1 Correlation between monometallic and bimetallic solutions

For each A_mB_n system, we shall apply the monometallic nanocluster design methodology from ref. 15 and compute the pool of the $P = 20$ best solutions and their corresponding dimensionless cohesive energies, $\overline{E^{coh}}$. These solutions represent different nanocluster shapes of size $m + n$ that we can now rank from one to twenty in terms of the above energies. Then, focusing on each of these shapes, one at a time, we solve the chemical ordering MILP model to obtain

corresponding optimal bimetallic designs and the associated cohesive energy values, E^{coh}, according to the bond-centric model. With these results at hand, we shall first investigate the extent to which the optimality of a cluster shape in the monometallic case correlates to the cohesiveness of bimetallic clusters.

Fig. 2a presents a histogram of the monometallic solution ranks from which the various best cohesive bimetallic designs were obtained. In other words, each bar in the histogram represents the count of A_mB_n systems for which the best (out of twenty) bimetallic clusters originated from a monometallic cluster shape (among the twenty such shapes) with a given rank (from the highest to the twentieth highest in terms of dimensionless cohesive energy). From this histogram, we can observe that around 80% of the best bimetallic designs can be derived from nanocluster shapes that ranked first in the monometallic solution pool. We can thus utilize the occurrence frequency of a given rank in this histogram to approximate the probability of generating an optimal bimetallic design from a monometallic solution of this rank. Since the occurrence frequency shows a general decreasing trend for all three chemistries of interest, we conclude that the probability of a given shape corresponding to the optimal bimetallic design decreases rapidly, as the monometallic optimality of a cluster shape decreases, while it is relatively unlikely that the optimal bimetallic cluster shape is not represented in one of the first four or five monometallic optimal shapes. This observation motivates our algorithmic choice of $P = 20$ as the size of the collection of monometallic clusters that are to be considered when initializing the search for optimal bimetallic designs.

We now seek to establish a direct quantitative metric of the correlation between $\overline{E^{coh}}$ and E^{coh}. To do so, we expand our focus to a total of 100 cluster shapes for each A_mB_n, consisting of the original $P = 20$ ranked ones as well as an additional 80 shapes obtained *via* the CPLEX code's solution pool facility applied on the monometallic nanocluster model from ref. 15. Following the previous procedure, we apply the chemical ordering MILP model and calculate E^{coh} for all resulting bimetallic clusters. These are then compared against the dimensionless cohesive energies of the monometallic clusters, $\overline{E^{coh}}$. With all A_mB_n systems we studied, we noticed generally positive correlations between $\overline{E^{coh}}$ and E^{coh}. Fig. 2b plots such correlations for an example composition of $A_{19}B_{18}$, for the three chemistries of interest. In particular, the AuAg clusters show a near perfect correlation with an R^2 value of 0.997, the AuCu clusters show strong correlation with an R^2 value of 0.921, while the CuAu system exhibits a relatively weaker correlation with an R^2 value of 0.558. We remark that similar correlation trends are observed for the other compositions The correlations between $\overline{E^{coh}}$ and E^{coh} suggest that, for the systems we have investigated, the shape of a bimetallic nanocluster plays a important role in determining its cohesive energy. Arguably,
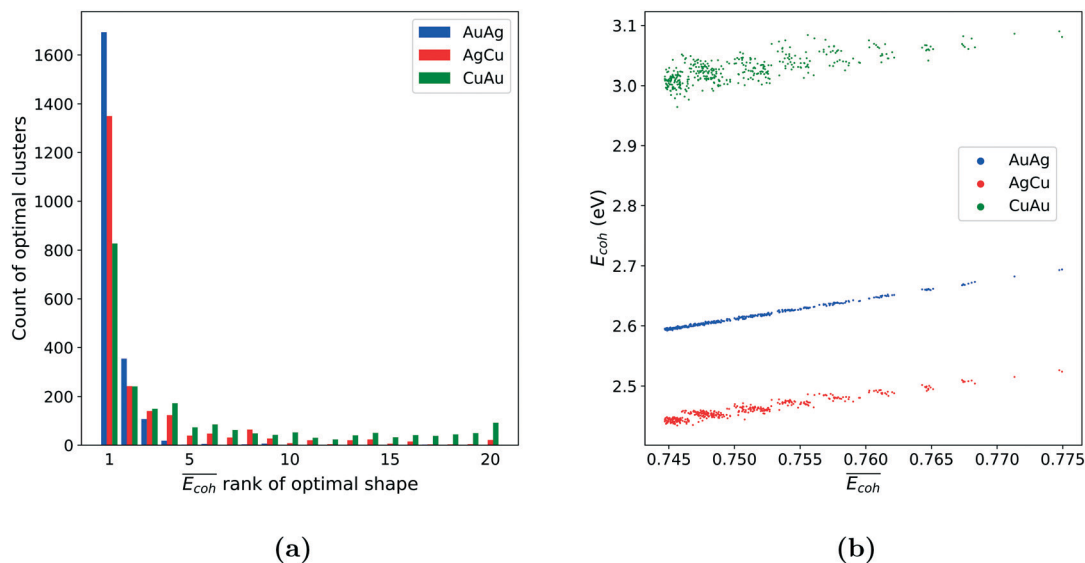
This journal is © The Royal Society of Chemistry and IChemE 2021

Mol. Syst. Des. Eng., 2021, **6**, 545–557 | 551

(a)

(b)

Fig. 2 (a) Histogram of $\overline{E^{coh}}$ ranks of optimal bimetallic cluster shapes. (b) Parity plot between $\overline{E^{coh}}$ and E^{coh} for representative test instances $Au_{19}Ag_{18}$, $Ag_{19}Cu_{18}$ and $Cu_{19}Au_{18}$.

a highly cohesive monometallic nanocluster shape is a good starting place for designing a highly cohesive bimetallic nanocluster, motivating our decision to pursue the proposed two-step solution strategy.

4.2 Improving designs *via* metaheuristic search

In this section, we discuss our computational experiments to validate the effectiveness of our purpose-built SA metaheuristic scheme for searching over the design space of nanocluster shapes. More specifically, we compare the cohesive energies of the best identified cluster before and after applying the two-step solution strategy. Furthermore, in order to validate the utility of applying the chemical ordering MILP at each step of the metaheuristic search, we also implemented a bare-bones version of the SA search whereby the repositioned surface atoms retain their atomic labels, skipping the chemical ordering step to relabel every atom of the new cluster. In the following, we refer to these two approaches as "SA-MILP" and "SA-only", respectively.

Fig. 3 presents example computational results for the case of 39-atom CuAu clusters, using a CPU time limit of 100 seconds in all cases. We should highlight that, just like many other metaheuristic algorithms, simulated annealing invokes a random number generator to decide whether any non-improving designs are accepted as part of the solution trajectory. To that end, in order to avoid any randomness effects due to the choice of the random number generator seed, the cohesive energies presented in this figure correspond to the best values among 10 runs of the SA process, each time utilizing a different seed for the random number generator.

The plot reveals that, compared to the initial solutions ("no SA") corresponding to shapes of monometallic nanoclusters, both the "SA-MILP" and "SA-only" approaches

help to improve solution quality. The improvements are most significant in composition ratios between 0.3 and 0.5, when the amounts of the two metals are comparable and where the combinatorial complexity is the greatest. In addition, we note that the "SA-MILP" approach tends to find better solutions than the "SA-only", suggesting that the MILP chemical ordering step indeed accelerates the search process. For example, focusing on the $Cu_{14}Au_{25}$ system (singled-out in Fig. 3), we notice that the best cluster considering only optimal orderings of monometallic nanocluster shapes (*i.e.*, the green dot) exhibits noticeably lower cohesiveness than what can be achieved by subjecting those structures to atom rearrangements *via* the SA search process (*i.e.*, the red dot), while with the integration of MILP-based chemical ordering
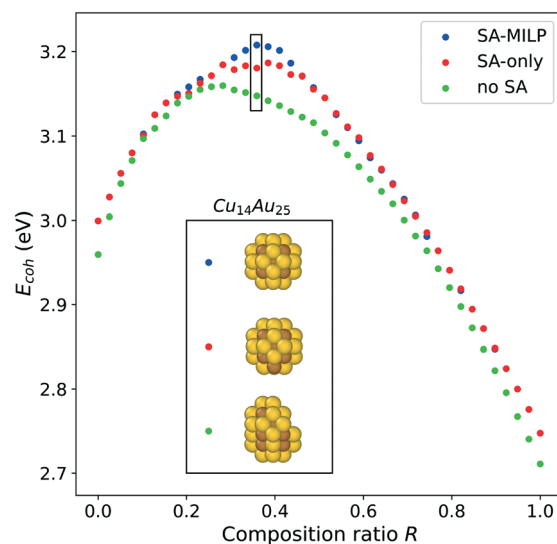

Fig. 3 Comparison of solutions obtained *via* different search strategies for representative clusters Cu_mAu_n with $m + n = 39$.

552 | *Mol. Syst. Des. Eng.*, 2021, **6**, 545–557

This journal is © The Royal Society of Chemistry and IChemE 2021

optimization at each step of the search, an even better structure is identified (*i.e.*, the blue dot). Noting that these results are representative of other instances we have tested, we conclude that our purpose-built SA-based algorithm to search over cluster shapes, combined with an MILP-based search over chemical orderings, constitutes an efficient strategy for designing highly cohesive, and hence stable, bimetallic nanoclusters. The optimality boost provided by the metaheuristic is especially helpful for systems with a relatively weaker $\overline{E^{coh}} - E^{coh}$ correlations, such as the CuAu case.

4.3 Trends among bimetallic solutions

The two-step methodology we presented in this paper is a powerful tool for systematically exploring the design space and understanding bimetallic nanoclusters' stability. The framework's most direct usage is to identify optimally stable designs for given sizes, compositions, and bimetallic systems. The obtained designs can then serve as model nano-structures for further experimental and theoretical investigations. At the same time, when considered collectively, the complete library of stable bimetallic nanoclusters can build intuition on how different factors interact and affect stability.

In our previous study on the stability of monometallic nanoclusters,[15] we observed that, as the particle size increases, its cohesive energy asymptotically approaches the bulk value but with noteworthy discontinuities of the trend at certain so-called magic numbers. In general, magic number effects may be arising in highly symmetrical structures and based on enhanced stability of their electronic structure. To investigate the size effect for bimetallic nanoclusters, we compare here results across various sizes of

the same specified compositions. As shown in Fig. 4a, a similar trend of asymptotically increasing cohesive energies applies. We also notice deviations from a purely monotonic increase at specific sizes and compositions (*e.g.*, CuAu system at $N = 10$), which may be explained by applicable magic number effects that are however far less understood in bimetallic systems.

With bimetallic nanoclusters, it is also important to investigate how composition affects their stability. Researchers are especially interested in minimum compositions of noble metal in catalysts[32] and magic compositions of additive or synergistic effects. To that end, we can scan our results library at given sizes and compare structures along various compositions. As Fig. 4b shows, among the three systems investigated, AuAg and AgCu show direct additive effects between their two metals in terms of cohesive energy, where adding atoms of higher bulk cohesion (Au and Cu, respectively) increases the particle's total cohesive energy linearly. In contrast, for the CuAu system, we observe nonlinear synergistic effects between those two metals, whereby mixed nanoclusters tend to have higher cohesive energy than their pure counterparts. More specifically, for the range of sizes represented in this plot, an most cohesive composition arises at approximately 40% Cu to Ag ratio where the highest cohesive energy is attained.

In addition to investigating optimal solutions in terms of the cohesive energy values, we can also study their structure features qualitatively. We are particularly interested in the segregation patterns exhibited by stable designs, because these patterns significantly affect catalytic reactivity and magnetic properties. In our studies, we observed that nearly all of the optimal solutions are quasi-spherical, and hence, we employ the mean distance to the geometric center (MDG) as a suitable metric for the level of segregation. For example,
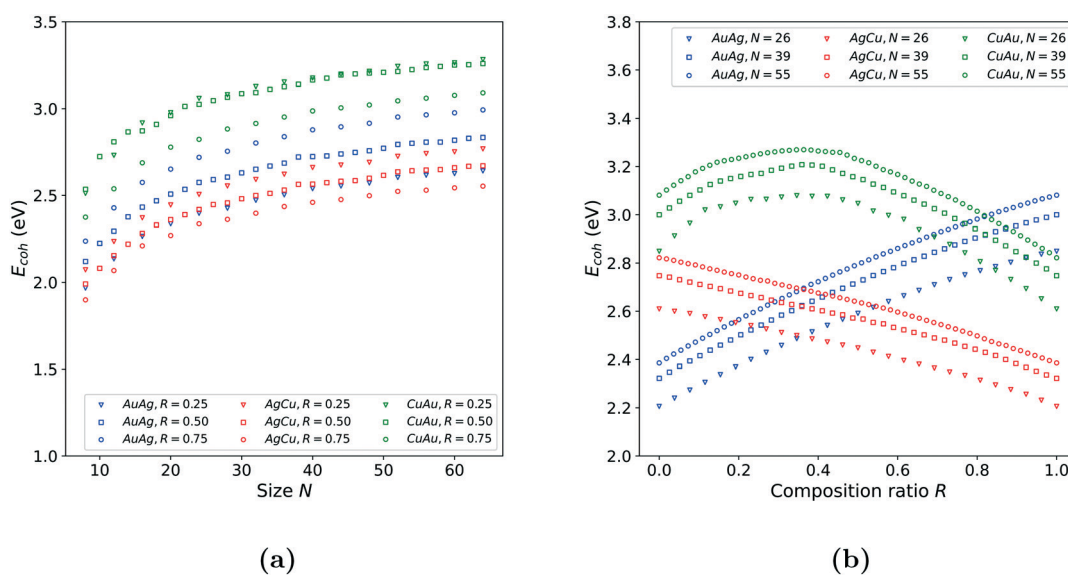

(a)   **(b)**

Fig. 4 Impact on optimal cohesive energies of bimetallic nanoclusters of (a) size N at three composition ratios $R \in$ {25%, 50%, 75%} (b) composition ratios R at three sizes $N \in$ {26, 39, 55}.
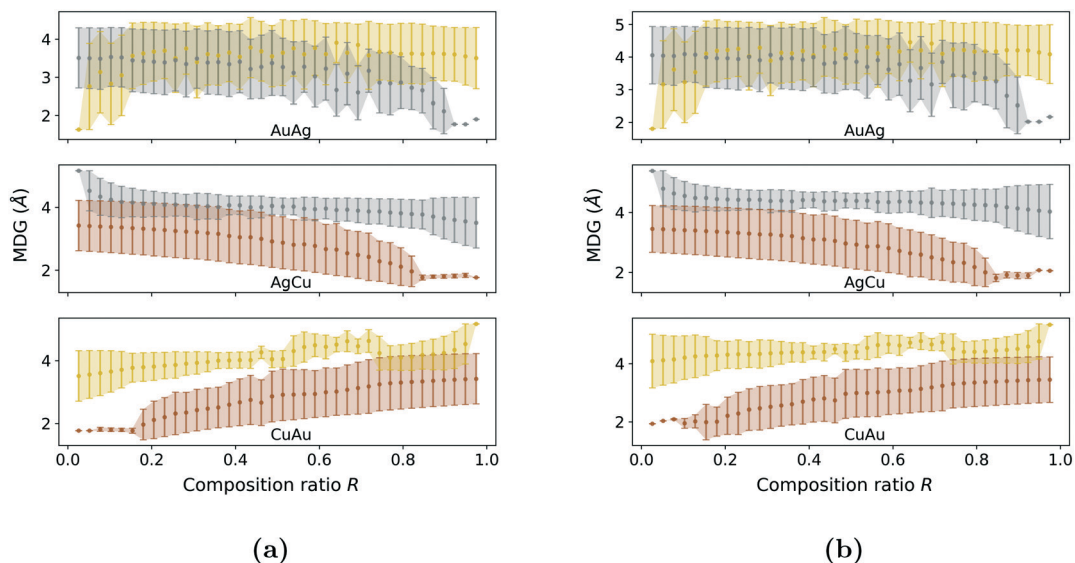
Fig. 5 MDG values and standard deviations for size N = 39 (a) FCC optimal designs, and (b) DFT-relaxed designs; gold, silver, and copper colors encode the respective metals.

if a certain type of atoms tends to segregate to the surface, then we should observe a divergence of the MDG of the two atom types in the cluster.
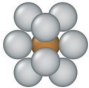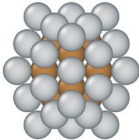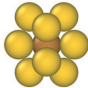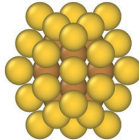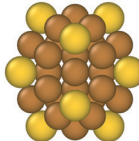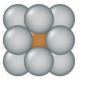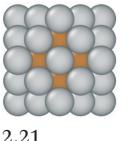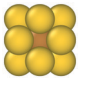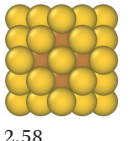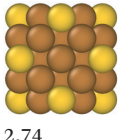
Fig. 5a reports MDG calculations for our optimal solutions across all composition ratios and for the representative cluster size N = 39. From these plots, we can clearly infer the corresponding segregation patterns. More specifically, in the CuAu system, the Au atoms tend to have larger MDG than the Cu atoms, indicating that the Au atoms tend to distribute at the surface, while the Cu atoms aggregate into the center of the particle. Similar trends also appear in the AgCu system, with the Ag atoms preferentially distributing at the surface. The AuAg system shows a more complicated pattern. When fewer Au atoms are in the particle, Ag atoms tend to have larger MDG values. However, as the number of Au atoms increases, the pattern shifts to having more Au atoms on the surface. Those observations suggest interesting configurations of optimally stable bimetallic nanoclusters. By inspecting detailed AgCu configurations more closely, we can note Cu@Ag core–shell structures for instances with a few Cu, when Ag tends to segregate to the surface. When more Cu atoms and a few Ag atoms exist in the particle, highly symmetric Cu-core Ag-decorated structures are identified. Similar configurations are observed in the CuAu system. It should be noted that those configurations are highly symmetric. For the AuAg system, Ag tends to segregate to the surface at low Au composition, while Au@Ag core–shell structures are observed. In contrast, at high Au composition, Au tends to segregate to the surface, and Ag@Au core–shell structures are found. These structural trends have been also observed on minimum-energy structures of larger bimetallic nanoparticles (sizes reaching 4000 atoms) by combining the bond-centric model with a genetic algorithm, where Cu resides in the core of AuCu and AgCu nanoparticles and AgAu particles show well-mixed behavior.[11] This could be

partially explained by the fact that the bulk cohesive energy value of copper is higher than that of silver and, hence, optimal designs tend to form many Cu–Cu bonds in the core. In general, the final designs result from an optimized trade-off between many factors, such as number of bonds, strength of bonds, and the overall geometry of the lattice.

Next, we attempt to validate that the structures obtained *via* our design approach retain their stability characteristics as well as the associated trends even when subjected to DFT relaxations. In order to apply DFT calculations, we note that there exists systematic deviations of *ab initio* calculated and experimental bulk cohesive energies, which are essential parameters in the bond-centric model. Thus, for a fair comparison, we feed the DFT-calculated key parameters to our methodologies. The identified optimal bimetallic configurations are then relaxed with DFT calculations. More specifically, for each structure, we pre-optimized by scaling the atomic coordinates to minimize the energy according to effective medium theory (EMT), as implemented in the atomic simulation environment (ASE).[33] A full DFT optimization was then carried out on the pre-optimized structure. We utilized CP2K[34,35] in conjunction with the PBE functional[36] and the DZVP basis sets of VandeVondele and Hutter,[37] along with the pseudopotentials of Goedecker, Teter, and Hutter[38] and a planewave cutoff of 500 Ry. The self-consistent field (SCF) procedure was converged to within 10^{-8} Ha, and geometries were optimized until forces were below 4.5×10^{-4} Ha per Bohr.

We then take the final DFT-relaxed structures and report their MDG values in Fig. 5b. As can be observed by comparing the respective MDG values, there exists a good quantitative agreement between the DFT-relaxed and FCC optimal solutions, while qualitatively, we also confirm the DFT-relaxed structures maintain the mixing patterns observed previously. We acknowledge that DFT optimization

Table 1 Comparison of optimal designs under cuboctahedron (FCC) and icosahedron geometries

Lattice	$Ag_{12}Cu_1$	$Ag_{42}Cu_{13}$	Cu_1Au_{12}	$Cu_{13}Au_{42}$	$Cu_{43}Au_{12}$
Icosahedron					
$E_{coh}^{ico}(eV)$	1.89	2.30	2.29	2.65	2.84
Cuboctahedron (FCC)					
$E_{coh}^{cub}(eV)$	1.76	2.21	2.17	2.58	2.74
$E_{coh}^{ico}/E_{coh}^{cub}$	1.07	1.04	1.05	1.03	1.04

is always contingent to the initial structure that is provided as input. However, if the optimization methodology would result to unrealistic bimetallic nanocluster designs, this should be depicted in the DFT optimization where significant cluster reconstruction should occur. Thus, Fig. 5b demonstrates that the clusters retain their structural trends after DFT optimization. These results further illustrate the ability of the two-step approach presented in this paper to yield bimetallic nanocluster structures that are indeed highly stable and that retain their general shape and associated segregation pattern under lattice relaxation.

4.4 Effect of lattice type on segregation patterns

Given our framework's amenability to consider various lattice types, we provide here a brief investigation of how the choice of lattice might affect the optimal chemical orderings and resulting segregation patterns expected in highly stable clusters. More specifically, we reran our chemical ordering optimization model on $N = 13$ and $N = 55$ perfect icosahedron enclosure shapes, for various compositions, and compared the results with the corresponding designs based on a cuboctahedron lattice (*i.e.*, FCC). As illustrated in Table 1, optimal orderings within icosahedral clusters show slightly higher cohesiveness than optimal orderings in their cuboctahedral counterparts. This can be explained by the fact that, for the same size, there are more bonds in icosahedral clusters than in cuboctahedral ones. Among the five example instances, $Ag_{12}Cu_1$ exhibits the highest cohesive energy ratio between icosahedron and cuboctahedron shapes, suggesting that, at this size and composition, the AgCu system has a greater tendency to form icosahedron shaped nanoclusters rather than FCC ones. Despite these absolute differences in cohesive energies, the optimal orderings are similar, exhibiting the same segregation patterns. For example, $Ag_{12}Cu_1$, $Ag_{42}Cu_{13}$, Cu_1Au_{12}, and $Cu_{13}Au_{42}$ all form core–shell structures with Cu cores, while highly symmetric Cu-core/Au-decorated structures of $Cu_{43}Au_{12}$ are observed, in both icosahedron and cuboctahedron shapes. Overall, the above analyses support the conclusion that the segregation patterns observed earlier in this paper for FCC clusters would not change significantly, if icosahedron shapes are in effect.

5 Conclusions

We have a rigorous design framework, hybridizing exact MILP-based and metaheuristic search optimization, for identifying highly stable bimetallic nanoclusters. To alleviate obvious tractability challenges when faced with a highly combinatorially complex design space such as those arising for bimetallic particles, we proposed a clever "structure-first-order-second" decomposition of the full design task into two steps, namely the optimization of the particle shape followed by the optimization of chemical ordering within a given shape. To that end, we applied simulated annealing to guide the search across nanocluster shapes, coupled with an MILP model to identify the optimal homotop associated with each nanocluster shape visited in the search trajectory.

In the course of our computational experiments, we obtained an excess of six thousand optimal solutions of AuAg, AgCu and CuAu nanoclusters with up to 65 atoms, demonstrating that our design framework can identify highly cohesive bimetallic nanocluster configurations. The latter can serve as model particles for further investigations, enabling the efficient and systematic exploration of their stability properties. Many unintuitive bimetallic configurations were obtained, including core–shell structures and symmetric core-decorated structures. We also looked at how size and composition affect a cluster's cohesion, revealing many interesting instances whereby alloyed clusters demonstrated greater cohesive energy than their monometallic counterparts. Furthermore, we observed various interesting segregation patterns that remained unaffected when submitting the clusters to DFT relaxations. Most notably, we confirmed that Cu atoms tend to segregate into the core in both AgCu and CuAu systems.

Conflicts of interest

There are no conflicts to declare.

This journal is © The Royal Society of Chemistry and IChemE 2021

Mol. Syst. Des. Eng., 2021, **6**, 545–557 | **555**

Acknowledgements

References

1 J. P. Wilcoxon and B. L. Abrams, Synthesis, structure and properties of metal nanoclusters, *Chem. Soc. Rev.*, 2006, **35**(11), 1162–1194.

2 K. D. Gilroy, A. Ruditskiy, H.-C. Peng, D. Qin and Y. Xia, Bimetallic nanocrystals: syntheses, properties, and applications, *Chem. Rev.*, 2016, **116**(18), 10414–10472.

3 R. Ferrando, Determining the equilibrium structures of nanoalloys by computational methods, *J. Nanopart. Res.*, 2018, **20**(7), 1–13.

4 F. H. Stillinger, Exponential multiplicity of inherent structures, *Phys. Rev. E: Stat. Phys., Plasmas, Fluids, Relat. Interdiscip. Top.*, 1999, **59**(1), 48.

5 R. Ferrando, J. Jellinek and R. L. Johnston, Nanoalloys: from theory to applications of alloy clusters and nanoparticles, *Chem. Rev.*, 2008, **108**(3), 845–910.

6 S. Darby, T. V. Mortimer-Jones, R. L. Johnston and C. Roberts, Theoretical study of cu–au nanoalloy clusters using a genetic algorithm, *J. Chem. Phys.*, 2002, **116**(4), 1536–1550.

7 A. R. Oganov and C. W. Glass, Crystal structure prediction using ab initio evolutionary techniques: Principles and applications, *J. Chem. Phys.*, 2006, **124**(24), 244704.

8 H. G. Kim, S. K. Choi and H. M. Lee, New algorithm in the basin hopping monte carlo to find the global minimum structure of unary and binary metallic nanoclusters, *J. Chem. Phys.*, 2008, **128**(14), 144702.

9 A. Granja-Delrio, H. A. Abdulhussein and R. L. Johnston, Dft-based global optimization of sub-nanometer ni–pd clusters, *J. Phys. Chem. C*, 2019, **123**(43), 26583–26596.

10 R. Jinnouchi and R. Asahi, Predicting catalytic activity of nanoparticles by a dftaided machine-learning algorithm, *J. Phys. Chem. Lett.*, 2017, **8**(17), 4279–4283.

11 J. Dean, M. J. Cowan, J. Estes, M. Ramadan and G. Mpourmpakis, Rapid prediction of bimetallic mixing behavior at the nanoscale, *ACS Nano*, 2020, **14**(7), 8171–8180.

12 C. L. Hanselman and C. E. Gounaris, A mathematical optimization framework for the design of nanopatterned surfaces, *AIChE J.*, 2016, **62**(9), 3250–3263.

13 C. L. Hanselman, W. Zhong, K. Tran, Z. W. Ulissi and C. E. Gounaris, Optimization-based design of active and stable nanostructured surfaces, *J. Phys. Chem. C*, 2019, **123**(48), 29209–29218.

14 C. L. Hanselman, D. R. Alfonso, J. W. Lekse, C. Matranga, D. C. Miller and C. E. Gounaris, *et al.* A framework for optimizing oxygen vacancy formation in doped perovskites, *Comput. Chem. Eng.*, 2019, **126**, 168–177.

15 M. N. Isenberg, M. G. Taylor, Z. Yan, C. L. Hanselman, G. Mpourmpakis and C. E. Gounaris, Identification of optimally stable nanocluster geometries via mathematical optimization and density-functional theory, *Mol. Syst. Des. Eng.*, 2020, **5**(1), 232–244.

16 F. L. Deepak, *Metal nanoparticles and clusters: Advances in synthesis, properties and applications*, Springer, 2017.

17 Z. Yan, M. G. Taylor, A. Mascareno and G. Mpourmpakis, Size-, shape-, and composition-dependent model for metal nanoparticle stability prediction, *Nano Lett.*, 2018, **18**(4), 2696–2704.

18 A. P. Sutton, *Electronic structure of materials*, Clarendon Press, 1993.

19 D. Tomanek, S. Mukherjee and K. H. Bennemann, Simple theory for the electronic and atomic structure of small clusters, *Phys. Rev. B: Condens. Matter Mater. Phys.*, 1983, **28**(2), 665.

20 J. K. Nørskov, T. Bligaard, F. Hvolbæk, F. Abild-Pedersen, I. Chorkendorff and C. H. Christensen, The nature of the active site in heterogeneous metal catalysis, *Chem. Soc. Rev.*, 2008, **37**(10), 2163–2171.

21 J. Dean, M. G. Taylor and G. Mpourmpakis, Unfolding adsorption on metal nanoparticles: Connecting stability with catalysis, *Sci. Adv.*, 2019, **5**(9), eaax5101.

22 R. Huang, J.-X. Bi, L. Li and Y.-H. Wen, Basin hopping genetic algorithm for global optimization of ptco clusters, *J. Chem. Inf. Model.*, 2020, **60**(4), 2219–2228.

23 I. B. M. Corporation, *IBM ILOG CPLEX Optimization Studio V12.9.0*, 2019.

24 X.-S. Yang, *Engineering optimization: An introduction with metaheuristic applications*, John Wiley & Sons, 2010.

25 X.-S. Yang, *Nature-inspired metaheuristic algorithms*, Luniver press, 2010.

26 C. Blum and A. Roli, Metaheuristics in combinatorial optimization: Overview and conceptual comparison, *ACM Comput. Surv.*, 2003, **35**(3), 268–308.

27 E.-G. Talbi, Combining metaheuristics with mathematical programming, constraint programming and machine learning, *Ann. Oper. Res.*, 2016, **240**(1), 171–215.

28 M. Fischetti and M. Fischetti, Matheuristics, in *Handbook of heuristics*, Springer, 2018, pp. 121–153.

29 K. A. Dowsland and J. Thompson, Simulated annealing, in *Handbook of natural computing*, 2012, pp. 1623–1655.

30 C. Kittel, *Introduction to Solid State Physics*, Wiley, New York, 8th edn, 2005.

31 M. D. Morse, Clusters of transition-metal atoms, *Chem. Rev.*, 1986, **86**(6), 1049–1109.

32 L. Liu and A. Corma, Metal catalysts for heterogeneous catalysis: from single atoms to nanoclusters and nanoparticles, *Chem. Rev.*, 2018, **118**(10), 4981–5079.

33 A. H. Larsen, J. J. Mortensen, J. Blomqvist, I. E. Castelli, R. Christensen, M. Dułak, J. Friis, M. N. Groves, B. Hammer and C. Hargus, *et al.* The atomic simulation environment|a python library for working with atoms, *J. Phys.: Condens. Matter*, 2017, **29**(27), 273002.

34 J. Hutter, M. Iannuzzi, F. Schiffmann and J. VandeVondele, cp2k: atomistic simulations of condensed matter systems, *Wiley Interdiscip. Rev.: Comput. Mol. Sci.*, 2014, **4**(1), 15–25.

35 J. VandeVondele, M. Krack, F. Mohamed, M. Parrinello, T. Chassaing and J. Hutter, Quickstep: Fast and accurate density functional calculations using a mixed gaussian and plane waves approach, *Comput. Phys. Commun.*, 2005, **167**(2), 103–128.

36 J. P. Perdew, K. Burke and M. Ernzerhof, Generalized gradient approximation made simple, *Phys. Rev. Lett.*, 1996, **77**(18), 3865.

37 J. VandeVondele and J. Hutter, Gaussian basis sets for accurate calculations on molecular systems in gas and condensed phases, *J. Chem. Phys.*, 2007, **127**(11), 114105.

38 S. Goedecker, M. Teter and J. Hutter, Separable dual-space gaussian pseudopotentials, *Phys. Rev. B: Condens. Matter Mater. Phys.*, 1996, **54**(3), 1703.

This journal is © The Royal Society of Chemistry and IChemE 2021

Mol. Syst. Des. Eng., 2021, **6**, 545–557 | **557**